Spin Transfer Torques in Ultra-Scaled MRAM Cells

M. Bendra*,**, S. Fiorentini*, J. Ender*,**, R.L. de Orio**, T. Hadámek*,
W.J. Loch*, N.P. Jørstad*, S. Selberherr**, W. Goes†, and V. Sverdlov*,**
* Christian Doppler Laboratory for Nonvolatile Magnetoresistive Memory and Logic at the
** Institute for Microelectronics, TU Wien, Gußhausstraße 27-29, A-1040 Wien, Austria
† Silvaco Europe Ltd., Cambridge, United Kingdom
e-mail: bendra@iue.tuwien.ac.at

***Abstract*—Modern magnetoresistive random access memory (MRAM) cells with single-digit nanometer diameters, utilize a combination of perpendicular interface-induced and shape-driven out-of-plane anisotropy in a free layer (FL) consisting of several ferromagnetic parts separated by tunnel barriers and/or nonmagnetic spacers. To accurately evaluate the torques acting in such a structure, we generalized the coupled spin and charge drift-diffusion transport approach to account for a number of tunnel barriers (TB) or spacers separating the elongated ferromagnetic pieces. The inclusion of the tunneling magnetoresistance effect is achieved by modeling the TB as a poor conductor with a conductivity locally dependent on the relative magnetization orientation of the ferromagnetic layers. The TB parameters are calibrated to reproduce the expected torque magnitudes in magnetic tunnel junctions (MTJ). To reproduce the spin transfer torques acting on a FL in a MTJs with several TBs and spacers, a special treatment of the spin current is proposed. In elongated FLs, position-dependent torques are present in the ferromagnetic pieces due to non-homogeneous magnetization. We show that, with the proposed approach, composite FLs with several TBs are treated on equal footing. Our simulations of the magnetization dynamics in composite elongated FLs agree well with recent experimental demonstrations of switching of ultra-scaled MRAM cells.**

***Keywords*—Spin Transfer Torques, Ultra-Scaled MRAM Cells, LLG, perpendicular magnetic anisotropy**

I. Introduction

Emerging nonvolatile spin-transfer torque (STT) magnetoresistive random access memories (MRAM) offer high speed, endurance and are attractive for stand-alone [1], embedded automotive [2], MCU and IoT [3] applications, frame buffer memory [4], and slow SRAM [5]. An MRAM cell consists of several layers, including a CoFeB reference layer (RL) and a free magnetic layer (FL) separated by an MgO tunnel barrier (TB) (Fig. 1 (a)), which form the MTJ. To increase the perpendicular magnetic anisotropy, the FL, typically composed of two CoFeB layers and a thin metal buffer, is interfaced with a second MgO layer [6]. Introducing more MgO layers [7] and elongating the FL allows to boost the perpendicular anisotropy even further, while reducing the FL diameter [8]. For accurate design of ultra-scaled MRAM cells (Fig. 1 (b)) it is paramount to generalize the traditional Slonczewski [9] approach applicable only to thin FLs to properly incorporate: (**i**) normal metal buffers; (**ii**) MgO barriers between the CoFeB layers, as well as the barrier between the RL and FL, and (**iii**) the torques acting on the textured magnetization near TBs in elongated ultra-scaled FLs.

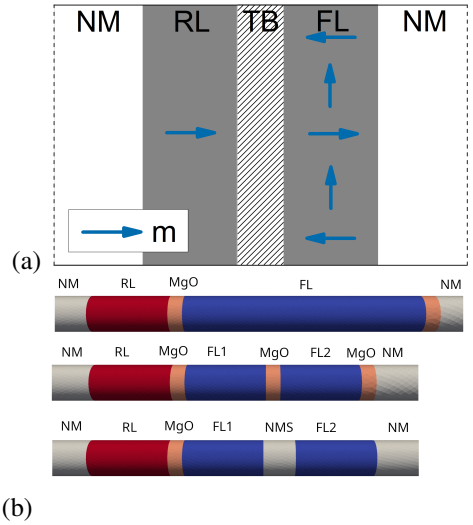

Fig. 1: (a) shows an MTJ with non-uniform FL magnetization, (b) shows examples of ultra-scaled MRAM cells.

II. Model

We developed a fully three-dimensional finite element method (FEM) based modeling and simulation approach which includes all physical phenomena, (described in equations (1)-(6)), which includes all physical phenomena, for proper ultra-scaled MRAM operation. We numerically solve the Landau-Lifshitz-Gilbert equation (LLG) (1) describing the magnetization dynamics

$$\frac{\partial \mathbf{m}}{\partial t} = -\gamma \mathbf{m} \times \mathbf{H}_{\text{eff}} + \alpha \mathbf{m} \times \frac{\partial \mathbf{m}}{\partial t} + \frac{1}{M_S} \mathbf{T_S} \quad (1)$$

$\mathbf{m} = \mathbf{M}/M_S$ is the position-dependent normalized magnetization, M_S is the saturation magnetization, α is the Gilbert damping constant, γ is the gyromagnetic ratio, and μ_0 is the vacuum permeability. The effective field $\mathbf{H}_{\text{eff}}$ includes the magnetic anisotropy field, the exchange, as well as the demagnetization fields. The latter contribution to $\mathbf{H}_{\text{eff}}$ is evaluated only on the disconnected magnetic domain by using a hybrid approach combining the boundary element method and the finite element method [10].

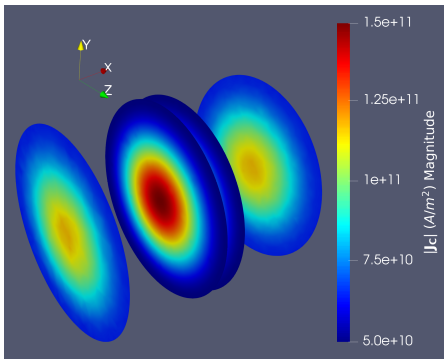

Fig. 2: Current density in an MTJ biased under a constant voltage for a non-uniform magnetization configuration of the FL, going from parallel in the center to anti-parallel on the side (c.f. Fig. 1 (a)).

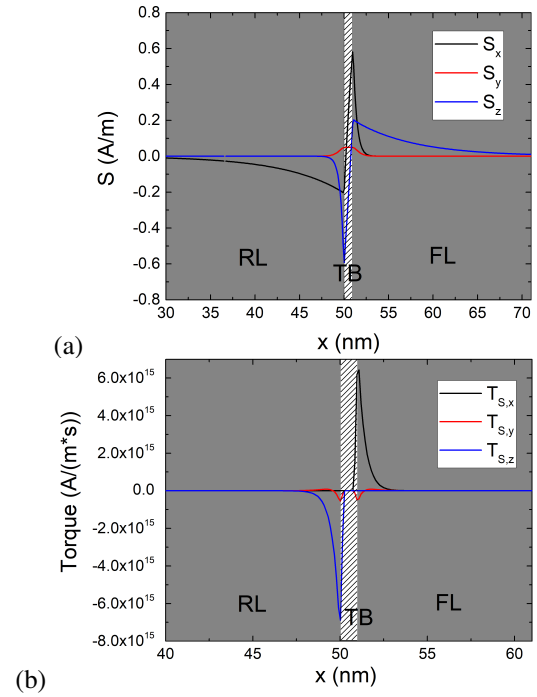

Fig. 3: Spin accumulation (a) and spin torque (b) solution with the spin-current boundary condition, semi-infinite ferromagnetic layers, $\lambda_J = 1\,\mathrm{nm}$ and $\lambda_\varphi = 0.4\,\mathrm{nm}$. The magnetization is along x in the RL and along z in the FL.

To appropriately model the switching of ultra-scaled MRAM cells the torque $\mathbf{T_S}$ has to be obtained by the following equation:

$$\mathbf{T_S} = -\frac{D_e}{\lambda_J^2}\mathbf{m}\times\mathbf{S} - \frac{D_e}{\lambda_\varphi^2}\mathbf{m}\times(\mathbf{m}\times\mathbf{S}). \qquad (2)$$

λ_J is the exchange length, λ_φ is the spin dephasing length, D_e is the electron diffusion coefficient in the ferromagnetic layers, and $\mathbf{S}$ is the coupled spin and charge transport. The coupled spin and charge drift-diffusion method, as defined by equations (3)-(5), accurately describes the charge and the spin transport through a nanometer sized magnetic valve [11].

$$D_e\left(\frac{\mathbf{S}}{\lambda_{sf}^2} + \frac{\mathbf{S}\times\mathbf{m}}{\lambda_J^2} + \frac{\mathbf{m}\times(\mathbf{S}\times\mathbf{m})}{\lambda_\varphi^2}\right) = -\boldsymbol{\nabla}\cdot\mathbf{J_S} \qquad (3)$$

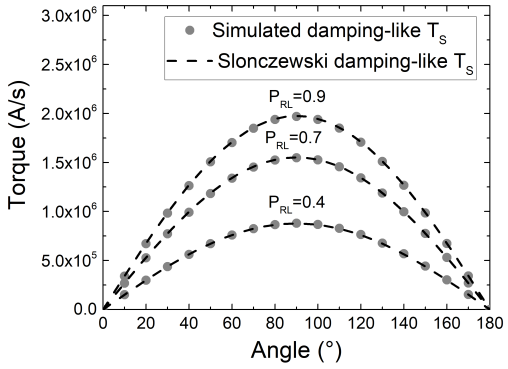

Fig. 4: Comparison of the angular dependence of the torque to the sinusoidal dependence predicted by [9].

$$\mathbf{J_S} = -\frac{\mu_B}{e}\beta_\sigma\big(\mathbf{J_C}\otimes\mathbf{m} + \beta_D D_e\frac{e}{\mu_B}[(\nabla\mathbf{S})\mathbf{m}]\otimes\mathbf{m}\big) - D_e\nabla\mathbf{S} \qquad (4)$$

$$\mathbf{J_C} = \sigma\mathbf{E} - \beta_D D_e\frac{e}{\mu_B}[(\boldsymbol{\nabla}\mathbf{S})\mathbf{m}] \qquad (5)$$

μ_B is the Bohr magneton, e is the electron charge, β_σ and β_D are polarization parameters. $\otimes$ is the outer product, $\mathbf{J_C}$ is the charge current density, and $\mathbf{J_S}$ is the spin current. We extended this method to MTJs by modeling the TB as a poor conductor (6) with a local resistance dependent on the relative orientation of the FL magnetization [12].

$$\sigma(\theta) = \frac{\sigma_P + \sigma_{AP}}{2}\left(1 + \left(\frac{\mathrm{TMR}}{2+\mathrm{TMR}}\right)\cos\theta\right) \qquad (6)$$

It is a manifestation of Ohm's law relating the voltage and the charge current through a structure with many transversal modes [11]. TMR tunneling magnetoresistance ratio, σ_P (σ_{AP}) is the conductivity in the P (AP) state, and θ is the local angle between the magnetic vectors in the free and reference layer. Fig. 2 shows the redistribution of the current density in an MTJ at a fixed voltage for the FL magnetization shown in Fig. 1 (a): the current density is larger in the center, where the FL magnetization is parallel to that of the RL and the magnetization-dependent conductivity is the highest.

The tunneling spin current polarization taken from [13] is introduced by applying appropriate magnetization dependent boundary conditions at the left and right interface of the tunneling layers.

III. Results

The spin accumulation and torques computed in a structure with semi-infinite ferromagnetic leads separated by a $1\,\mathrm{nm}$ thick tunnel junction are shown in Fig. 3. The transverse spin dephasing length is $\lambda_\varphi = 0.4\,\mathrm{nm}$, the exchange length is $\lambda_J = 1\,\mathrm{nm}$ and the spin-flip length is $\lambda_{sf} = 10\,\mathrm{nm}$. The small value of the dephasing length is in agreement with values in MTJs [14]. The tunneling spin current polarization creates a jump between the values of the spin accumulation at the left and right interface of the TB. This is the manifestation of the MTJ

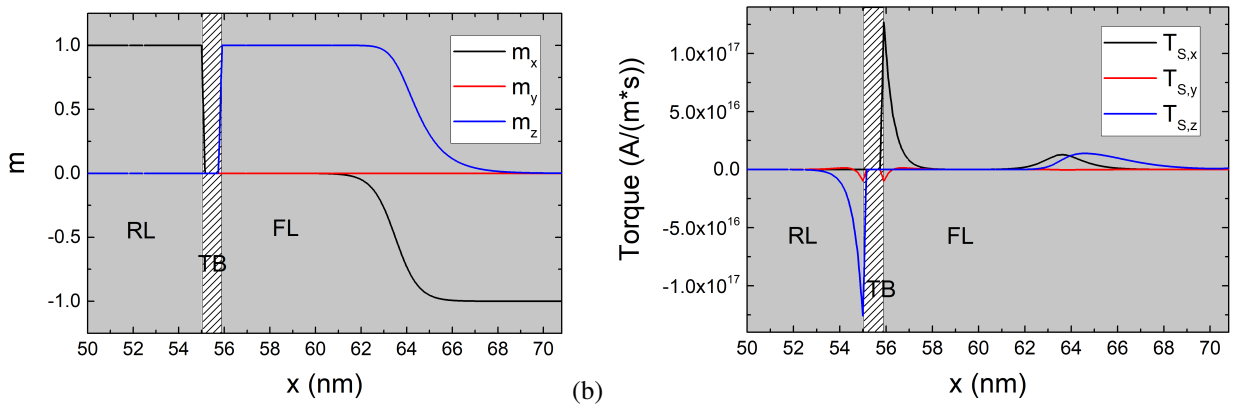

Fig. 5: Magnetization texture in an MTJ with elongated FL (a) and torques computed in the structure (b).

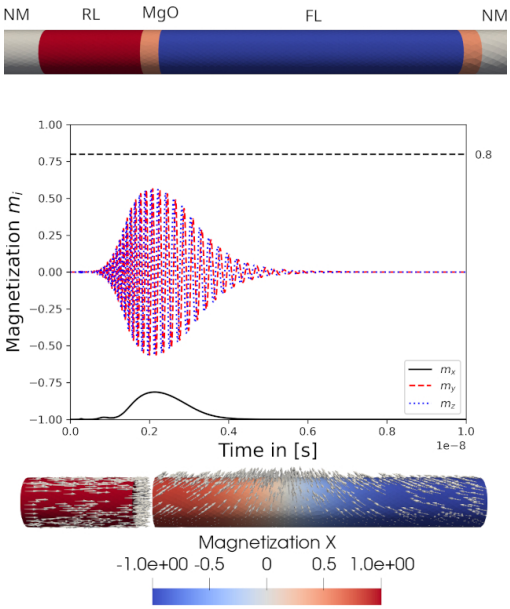

Fig. 6: An MRAM cell with 5 nm RL and an elongated 15 nm FL interfaced by two TB of 0.9 nm. At −1.5 V bias voltage applied, no switching occurs due to the formation of a domain wall as evidenced by the switching snapshot at 2 ns (bottom).

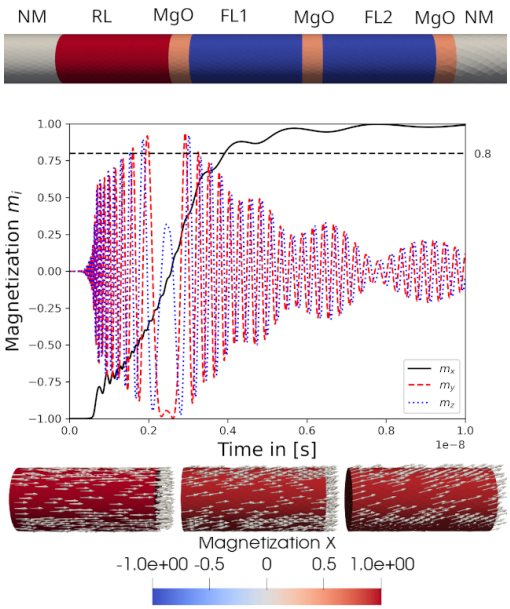

Fig. 7: Switching of an MRAM cell made of 5 nm RL, 0.9 nm TB, and composite FL separated by a 0.9 nm MgO layer. The FL consists of two ferromagnetic parts of 5 nm separated by a 0.9 nm MgO layer. The bias voltage is −1.5 V. A switching magnetization level of 0.8 is achieved after 4 ns. Damped oscillations after the switching are caused by the not completely aligned magnetizations of FL1 and FL2 relaxing to an equilibrium parallel position (bottom).

polarization effects on the spin current. The transverse spin accumulation is quickly absorbed, resulting in torques that are acting near the TB|FL interface.

In Fig. 4, the angular dependence of the torque acting on a semi-infinite FL is compared with the Slonczewski expression [9]. The sinusoidal angular dependence of the torque in an MTJ predicted by [9] is reproduced exactly, for semi-infinite and 2 nm thin ferromagnetic layers, and for various values of the RL|TB interface spin polarization. For a fixed voltage, the torque is independent of the TB|FL polarization.

The magnetization in elongated FLs of ultra-scaled MRAM is highly nonuniform during switching. A domain wall (DW) is created, which may propagate through the FL or dissolve. The torques acting in the presence of magnetization domain walls can be modeled by the Zhang and Li expression [15]. The advantage of the proposed approach when applied to ultra-scaled MRAM devices is the possibility of computing all sources of torque via a unified formalism. We compute the torque in an experimental MTJ structure [8] with a 5 nm RL, 0.9 nm TB, and an elongated FL of 15 nm, with the magnetization profile shown in (Fig. 5 (a)). The torque computed by the solver is displayed in (Fig. 5 (b)). Both the Slonczewski torque acting near the interface and the bulk torque due to the magnetization texture are simultaneously reproduced using a unique set of equations, showing the capability of the drift-diffusion approach to accurately describe the torque and switching in ultra-scaled MRAM.

Fig. 6 to Fig. 8 demonstrate the magnetization dynamics in ultra-scaled MRAM cells with a diameter of 2.3 nm, studied experimentally in [8], under −1.5 V bias voltage.

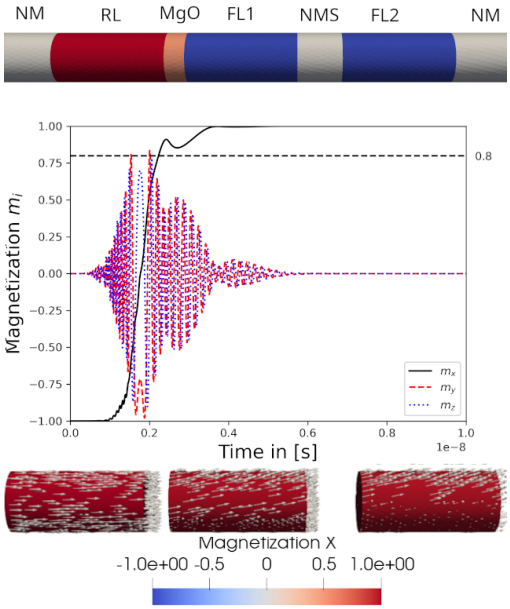

Fig. 8: Switching of an MRAM cell made of 5 nm RL, 0.9 nm TB, and composite FL separated by a 0.9 nm MgO layer. The FL consists of two ferromagnetic parts of 5 nm separated by a 2 nm non-magnetic spacer. The bias voltage is −1.5 V. A switching magnetization level of 0.8 is achieved after 2 ns, at which the MRAM cell is considered switched. Damped oscillations after the switching are caused by the not completely aligned magnetizations of FL1 and FL2 relaxing to an equilibrium parallel position (bottom).

The FLs are elongated to stabilize the perpendicular orientation with the help of the shape anisotropy. Shortly after the voltage is applied, a DW is formed in the 15 nm long FL (Fig. 6). The DW dissolves after $\sim$ 3 ns with the magnetization returning close to the starting position. The DW formation thus prevents the magnetization from switching. In contrast, if the FL is composed of two 5 nm long parts separated by an MgO layer (Fig. 7) or by a non-magnetic spacer (Fig. 8), the magnetization of FL1 is reverted first followed by the FL2 magnetization reversal due to the STT and the strong magnetostatic coupling between the FL1 and FL2. The whole FL switches successfully, in agreement with [8].

IV. Conclusion

We presented a successful design approach to accurately describe the charge and spin currents, the torques and the magnetization dynamics in ultra-scaled MRAM cells consisting of several elongated pieces of ferromagnets separated by multiple tunnel barriers. We demonstrated how the Slonczewski and Zhang and Li torques can be computed using a unified model, correctly describing the torques on textured magnetization in elongated FLs with several MgO TBs. The predictions from our design method agree well with the recent experimental demonstrations of switching of ultra-scaled MRAM cells, which rely not only on interface anisotropy, but also on shape anisotropy to achieve large perpendicular magnetic anisotropy.

Acknowledgment

The financial support by the Austrian Federal Ministry for Digital and Economic Affairs, the National Foundation for Research, Technology and Development and the Christian Doppler Research Association is gratefully acknowledged.

References

[1] S. Aggarwal, H. Almasi, M. DeHerrera, B. Hughes, S. Ikegawa *et al.*, "Demonstration of a reliable 1 Gb standalone spin-transfer torque MRAM for industrial applications," in *2019 IEEE International Electron Devices Meeting (IEDM)*, 2019, pp. 2.1.1–2.1.4.

[2] V. B. Naik, K. Yamane, T. Lee, J. Kwon, R. Chao *et al.*, "Jedec-qualified highly reliable 22nm FD-SOI embedded MRAM for low-power industrial-grade, and extended performance towards automotive-grade-1 applications," in *2020 IEEE International Electron Devices Meeting (IEDM)*, 2020, pp. 11.3.1–11.3.4.

[3] Y.-C. Shih, C.-F. Lee, Y.-A. Chang, P.-H. Lee, H.-J. Lin *et al.*, "A reflow-capable, embedded 8Mb STT-MRAM macro with 9ns read access time in 16nm FinFET logic CMOS process," in *2020 IEEE International Electron Devices Meeting (IEDM)*, 2020, pp. 11.4.1–11.4.4.

[4] S. H. Han, J. M. Lee, H. M. Shin, J. H. Lee, K. S. Suh *et al.*, "28-nm 0.08 nm^2/Mb embedded MRAM for frame buffer memory," in *2020 IEEE International Electron Devices Meeting (IEDM)*, 2020, pp. 11.2.1–11.2.4.

[5] J. Alzate, U. Arslan, P. Bai, J. Brockman, Y. J. Chen *et al.*, "2 MB array-level demonstration of STT-MRAM process and performance towards L4 cache applications," in *2019 IEEE International Electron Devices Meeting (IEDM)*, 2019, pp. 2.4.1–2.4.4.

[6] H. Sato, M. Yamanouchi, S. Ikeda, S. Fukami, F. Matsukura, and H. Ohno, "MgO/CoFeB/Ta/CoFeB/MgO recording structure in magnetic tunnel junctions with perpendicular easy axis," *IEEE Transactions on Magnetics*, vol. 49, no. 7, pp. 4437–4440, 2013.

[7] K. Nishioka, H. Honjo, S. Ikeda, T. Watanabe, S. Miura *et al.*, "Novel quad interface MTJ technology and its first demonstration with high thermal stability and switching efficiency for STT-MRAM beyond 2Xnm," in *2019 Symposium on VLSI Technology*, 2019, pp. T120–T121.

[8] B. Jinnai, J. Igarashi, K. Watanabe, T. Funatsu, H. Sato *et al.*, "High-performance shape-anisotropy magnetic tunnel junctions down to 2.3 nm," in *2020 IEEE International Electron Devices Meeting (IEDM)*, 2020, pp. 24.6.1–24.6.4.

[9] J. C. Slonczewski, "Currents, torques, and polarization factors in magnetic tunnel junctions," *Phys. Rev. B*, vol. 71, p. 024411, 2005.

[10] J. Ender, M. Mohamedou, S. Fiorentini, R. Orio, S. Selberherr, W. Goes, and V. Sverdlov, "Efficient demagnetizing field calculation for disconnected complex geometries in STT-MRAM cells," in *2020 International Conference on Simulation of Semiconductor Processes and Devices (SISPAD)*, 2020, pp. 213–216.

[11] C. Petitjean, D. Luc, and X. Waintal, "Unified drift-diffusion theory for transverse spin currents in spin valves, domain walls, and other textured magnets," *Phys. Rev. Lett.*, vol. 109, p. 117204, 2012.

[12] S. Fiorentini, J. Ender, S. Selberherr, R. de Orio, W. Goes, and V. Sverdlov, "Coupled spin and charge drift-diffusion approach applied to magnetic tunnel junctions," *Solid-State Electronics*, vol. 186, p. 108103, 2021.

[13] M. Chshiev, A. Manchon, A. Kalitsov, N. Ryzhanova, A. Vedyayev *et al.*, "Analytical description of ballistic spin currents and torques in magnetic tunnel junctions," *Phys. Rev. B*, vol. 92, p. 104422, 2015.

[14] K. Y. Camsari, S. Ganguly, D. Datta, and S. Datta, "Physics-based factorization of magnetic tunnel junctions for modeling and circuit simulation," in *2014 IEEE International Electron Devices Meeting*, 2014, pp. 35.6.1–35.6.4.

[15] S. Zhang and Z. Li, "Roles of nonequilibrium conduction electrons on the magnetization dynamics of ferromagnets," *Phys. Rev. Lett.*, vol. 93, p. 127204, 2004.